Near-Edge X-ray Absorption Fine Structure within Multilevel Coupled Cluster theory

Rolf H. Myhre,[†,¶] Sonia Coriani,[*,‡,§] and Henrik Koch[*,†,¶]

†*Department of Chemistry, Norwegian University of Science and Technology, 7491 Trondheim, Norway*

‡*Dipartimento di Scienze Chimiche e Farmaceutiche, Università degli Studi di Trieste, I-34127, Italy*

¶*Department of Chemistry and the PULSE Institute, Stanford University, Stanford, California 94305, USA*

§*Aarhus Institute of Avanced Studies, University of Aarhus, DK-8000 Århus C, Denmark*

E-mail: coriani@units.it; henrik.koch@ntnu.no

Abstract

Core excited states are challenging to calculate mainly because they are embedded in a manifold of high energy valence-excited states. Their locality, however, makes their determination ideal for local correlation methods. In this paper, we demonstrate the performance of multi-level coupled cluster theory in computing core spectra both within the core-valence separated and the asymmetric Lanczos implementations of coupled cluster linear response theory. A visualization tool to analyze the excitations based on the difference between the ground and excited state electron densities is also proposed.

1 Introduction

X-ray absorption spectroscopy (XAS) is a fundamental spectroscopic method for determining the electronic and structural properties of molecules, as well as their dynamic behavior.[1–7] In this type of spectroscopy, core electrons are excited, leaving behind a core hole. Since core orbitals are highly local, probing them yields important information about their local environment in the molecular system. An essential component for disclosing such information is the availability of computational methods to model the experimental spectra.

The calculation of core excitations using electronic structure theory encounters specific challenges not present for valence excitations. At the typical energies involved in X-ray spectroscopy, there is a high density of excited states with more loosely bounded electrons. These states form a continuum and the challenge is to obtain the core excited state within this continuum of states. Electronic structure programs usually employ subspace algorithms such as the Davidson algorithm[8,9] to determine eigenvalues. These methods are biased towards the lowest excitation energies, which makes their common implementations impractical for finding the high-energy excited states in question.

Due to the significant reduction in the screening of the nucleus following core excitation, relaxation effects play an essential role and need to be accounted for in a reliable manner. These relaxation effects mainly affect the molecular system in two ways: a direct, attractive effect contracting the valence electron density and an indirect repulsive effect from the interaction between the excited electron and the valence electrons which increases polarization. Additional issues that must be considered include the choice of basis set, the effect of relativity, vibrational effects and spectral broadening schemes.

Despite such difficulties, many methods have been presented to compute core spectra. More than forty years ago, Slater proposed the transition state method.[10,11] In this method, the molecular orbitals involved in the excitations are set to half occupation and the excitation energies are calculated as the difference between orbital energies. A somewhat similar method is the transition potential method where excitation energies are calculated from the derivative

of the total energy with respect to the occupation number when the occupations are set to one half in the relevant orbitals.[12,13] Another early approach is the multiple scattering or KKR[14–16] method. It describes electron propagation with a reference Green's function and a series of scattering events.

Density functional theory (DFT) based methods are the most common methods used to obtain core excitations and we will mention some of them here. One approach employs pseudopotentials, commonly used to describe core electrons and incorporate relativistic effects in DFT methods.[17] Pseudopotentials can be extended to include core holes, allowing the calculation of high energy excitations.[18] In the DFT variant of the ΔSCF method,[19] the electron density corresponding to Kohn-Sham orbitals is subtracted and added in each step of the self consistent iteration. Core excitations are then be obtained by subtracting the density corresponding to a core hole.[20] Other methods are based on time-dependent DFT (TDDFT). Examples are the complex propagator approach (CPP) of Norman and coworkers,[21,22] and the TDDFT method with a restricted excitation manifold.[23–25] In the CPP approach,[21,22] the absorption cross section of the core excitation process is obtained directly from scanning the imaginary part of the complex dipole polarizability over the relevant frequency region. The restricted excitation manifold methods are similar in spirit to the core-valence separation (CVS) technique.[26]

The core-valence separation is used in most wave-function-based methods for calculating X-ray excitations. Due to the large energy difference between the valence and core excited states, core-valence interaction parts of the Hamiltonian are very small and can be neglected.[26] The CVS approximation was first implemented within the second-order algebraic diagrammatic construction ADC(2)[27] method. Wenzel *et al.*[28–31] recently proposed it for the ADC(2), ADC(2)-x and ADC(3) hierarchy of methods based on the intermediate state representation variant of the ADC formalism.[32,33] Calculating excited states in ADC requires solving an eigenvalue problem for a secular matrix.[32,33] The core-valence separation greatly simplifies the eigenvalue problem by making the core excitations extremal eigenvalues

and significantly reducing the size of the vector space.

The calculation of X-ray absorption spectra has also been implemented within coupled cluster (CC) theory.[34–41] As in ADC, computing excited states in CC theory requires solving an eigenvalue problem, specifically the eigenvalues of the Jacobian. To obtain the eigenvalues corresponding to core excited states, an asymmetric Lanczos algorithm was used in Refs. 35 and 36 to construct a truncated tridiagonal representation of the Jacobian matrix. Diagonalization of this matrix makes it possible to obtain a full spectrum which includes core excitations.

It is well known that the Lanczos algorithm is numerically unstable and may require explicit biorthogonalization.[42] This makes it necessary to store and read a large number of vectors from disk, which becomes prohibitive for systems with more than 300 orbitals. For this reason, the CVS approximation has recently been implemented for CC linear response (CCLR) theory both within the Lanczos algorithm, and for conventional CCLR.[39] Alternative algorithms targeting X-ray excitations within the CC formalism are the CC-CPP approach,[40] and the energy-specific EOM-CC approach of Peng *et al.*[41] With the CVS approximation, the cost of calculating core excited states is approximately the same as the calculation of valence excited states and the bottleneck is the steep scaling of the CC methods with the dimension of the molecular system.

The locality of core excitations makes their calculation suitable for local methods such as the multi-level coupled cluster (MLCC) approach.[43,44] The MLCC method treats a small part of the molecular system with a high accuracy CC method and the rest of the system more approximately.[43,44] In this paper we test the capability of the multi-level CCSD (MLCCSD) approach to reproduce full CCSD Near Edge X-ray Absorption Fine Structure (NEXAFS) spectra. We compare spectra obtained both with the full space or regular Lanczos algorithm and with the Davidson algorithm with the CVS approximation.

In order to visualize and investigate the local nature of the excitations, ground and excited state one-electron densities are calculated and the corresponding orbital populations

are generated. The difference in the electron densities is then plotted and a visualization of the excitation process is obtained.

The paper is organized as follows. In the next section we give a brief outline of how to compute core spectra within the MLCC approach. Section 3 presents the results of some example calculations and the last section contains our concluding remarks.

2 Theory

2.1 Computing spectra within CC linear response theory

The CC wave function ansatz for a closed-shell system is defined by the exponential parametrization

$$|\mathrm{CC}\rangle = \exp(X)\,|\mathrm{HF}\rangle \tag{1}$$

where $|\mathrm{HF}\rangle$ is the Hartree-Fock reference state and $X = \sum_\mu x_\mu \tau_\mu$ is the cluster operator with the cluster amplitudes x_μ and the corresponding excitation operators τ_μ. Note that in conventional CC theory the cluster operator and amplitudes are usually written as T and t_μ, respectively. Here we use a slightly different notation because the symbols T and t_μ are reserved for the active space cluster operator and amplitudes in MLCC theory,[43,44] see also Section 2.3. The ground state energy and amplitudes are determined by projection of the Schrödinger equation on the reference state and a manifold of excitations

$$E = \langle \mathrm{HF}|\exp(-X) H \exp(X)\,|\mathrm{HF}\rangle \tag{2}$$

$$\Omega_\mu = \langle \mu|\exp(-X) H \exp(X)\,|\mathrm{HF}\rangle = 0\ . \tag{3}$$

In CC linear response theory, excitation energies, ω_k, and left, $\mathbf{L}_k$, and right, $\mathbf{R}_k$, excita-

tion vectors are usually obtained solving the asymmetric eigenvalue equations

$$\mathbf{A}\mathbf{R}_k = \omega_k \mathbf{R}_k; \quad \mathbf{L}_k\mathbf{A} = \omega_k \mathbf{L}_k \tag{4}$$

with the biorthogonality condition $\mathbf{L}_i\mathbf{R}_k = \delta_{ik}$. The Jacobian matrix $\mathbf{A}$ in Eq. (4) is defined as the derivative

$$A_{\mu\nu} = \frac{\partial \Omega_\mu}{\partial x_\nu} = \langle \mu | \exp(-X)[H, \tau_\nu] \exp(X) | \mathrm{HF} \rangle \tag{5}$$

Transition strengths for dipole components A and B are determined from the single residues of the linear response function, and take the form

$$S^{AB}_{0\to j} = \frac{1}{2}\left\{ \mathcal{M}^A_{0j}\mathcal{M}^B_{j0} + (\mathcal{M}^B_{0j}\mathcal{M}^A_{j0})^* \right\} \tag{6}$$

where the left and right transition moments are given by

$$\mathcal{M}^A_{0j} = \boldsymbol{\eta}^A \mathbf{R}_j + \bar{\mathbf{M}}^j(\omega_j)\boldsymbol{\xi}^A; \quad \mathcal{M}^B_{j0} = \mathbf{L}_j \boldsymbol{\xi}^B \tag{7}$$

and the auxiliary Lagrangian multipliers $\bar{\mathbf{M}}^j(\omega_j)$ are obtained from the solution of the linear equation

$$\bar{\mathbf{M}}^j \left(\mathbf{A} + \omega_j \mathbf{I}\right) = -\mathbf{F}\mathbf{R}_j. \tag{8}$$

We refer to Refs. 45 and 46 for the definition of the remaining building blocks.

Equation (4) is most often solved iteratively via some generalization of the Davidson algorithm.[8,9] The iterative procedure is initiated by selecting unit vectors corresponding to specific occupied to virtual orbital excitations, often based on Hartree-Fock orbital energy differences. The procedure will converge towards the lowest eigenvalues and eigenvectors even if the initial start vectors correspond to high energy excitations. This makes the procedure ill-suited for core excitations.

Another way to solve Eq. (4) is to build a tridiagonal representation, $\mathbf{T}$, of the Jacobian matrix $\mathbf{A}$ using an asymmetric Lanczos algorithm. The nonzero elements of the tridiagonal matrix $\mathbf{T} = \mathbf{P}^T\mathbf{A}\mathbf{Q}$ are given by

$$T_{ll} = \alpha_l = \mathbf{p}_l^T \mathbf{A} \mathbf{q}_l \tag{9}$$

$$T_{l+1,l} = \beta_l = \sqrt{\mathbf{p}_{l+l}^T \mathbf{q}_{l+1}} \tag{10}$$

$$T_{l,l+1} = \gamma_l = \mathrm{sgn}\{\mathbf{p}_{l+1}^T \mathbf{q}_{l+1}\}\beta_l \tag{11}$$

with the biorthogonal $\mathbf{p}_l$ and $\mathbf{q}_l$ vectors given by

$$\mathbf{q}_{l+1} = \beta_l^{-1}(\mathbf{A}\mathbf{q}_l - \gamma_{l-1}\mathbf{q}_{l-1} - \alpha_l \mathbf{q}_l) \tag{12}$$

$$\mathbf{p}_{l+1}^T = \gamma_l^{-1}(\mathbf{p}_l^T\mathbf{A} - \beta_{l-1}\mathbf{p}_{l-1}^T - \alpha_l \mathbf{p}_l^T). \tag{13}$$

It is neither necessary nor convenient to generate the full tridiagonal matrix $\mathbf{T}$, and the procedure can be truncated at some dimension $J \ll n$ where n is the dimension of the full Jacobian. The diagonalization of $\mathbf{T}$ produces an effective spectrum that covers the entire frequency range and converges from the top and bottom with increasing Lanczos chain length J.[36,47,48]

A convenient choice of start vectors for the Lanczos algorithm is

$$\mathbf{q}_1 = u_A^{-1}\boldsymbol{\xi}^A = \frac{\boldsymbol{\xi}^A}{||\boldsymbol{\xi}^A||}; \qquad \mathbf{p}_1^T = v_A^{-1}\boldsymbol{\eta}^A = \frac{||\boldsymbol{\xi}^A||}{\boldsymbol{\eta}^A\boldsymbol{\xi}^A}\boldsymbol{\eta}^A. \tag{14}$$

With this choice, the eigenvectors $\mathbf{L}$ and $\mathbf{R}$ of $\mathbf{T}$ form the basis for an approximate diagonal representation of the (complex) linear response function.[35,36] The absorption cross-section can then be computed from its imaginary component.[35,36] Moreover, one may compute directly the transition strengths as

$$S_{0\to j}^{AA} = u_A v_A L_{j1} R_{1j} - v_A^2 \sum_l \frac{L_{j1}L_{l1}\mathcal{F}_{lj}}{(\omega_j + \omega_l)} \quad , \tag{15}$$

see Refs. 35 and 36 for further definitions and details.

2.2 The core-valence separation

The CVS approximation can be implemented within both the Davidson and the asymmetric Lanczos algorithms.[39] Initially, a set of one or more core orbitals is selected. In each iteration of the solver, a projector $\mathcal{P}^v$ is applied on the trial vectors, removing all elements not referencing at least one of the selected core orbitals. For a singles and doubles trial vector, $\mathbf{b}$, the effect of the projector is

$$\begin{cases} \mathcal{P}^v b_i^a = 0 \quad \forall\ i = \text{valence}, \\ \mathcal{P}^v b_{ij}^{ab} = 0 \quad \forall\ i,j = \text{valence} \end{cases} \tag{16}$$

For the Davidson algorithm, Eq (4) becomes the projected eigenvalue equation

$$\mathcal{P}^v(\mathbf{A}\mathcal{P}^v\mathbf{R}_k) = \omega_k \mathcal{P}^v \mathbf{R}_k, \tag{17}$$

and similarly for the left eigenvectors. By applying the projector in each iteration during the solution of Eq. (8), the computation of CVS-CC transition moments and transition strengths is also easily obtained.

Within the Lanczos algorithm, the projector is applied during the iterative construction of the $\mathbf{T}$ matrix, i.e. to the $\mathbf{p}_l^T$ and $\mathbf{q}_l$ vectors and their linear transformations, $\mathbf{p}_l^T\mathbf{A}$ and $\mathbf{A}\mathbf{q}_l$. The resulting Lanczos eigenvectors, as well as the Lanczos trial vector bases, $\mathbf{P}^T$ and $\mathbf{Q}$, only contain excitations involving at least one core orbital. This effectively decouples them from excitations with contributions from occupied valence orbitals only. Diagonalization of the tridiagonal matrix yields the core excitations as lowest roots and quickly converges to the exact results with a significantly smaller Lanczos chain lengths. The oscillator strengths and cross sections are obtained without further modifications to the general procedure.

2.3 Multi-level coupled cluster theory for core spectra

Multi-level coupled cluster theory divides the molecular system into an active and an inactive part. By treating the active part with a highly accurate method and the inactive part more approximately, high accuracy results can be achieved at greatly reduced cost.[43,44] For example, the most expensive term in CCSD[49] scales as V^4O^2 where V and O are the number of virtual and occupied orbitals respectively. By dividing the system into an active CCSD part and an inactive part described by CC2,[50] one obtains the MLCCSD model. In this model, the scaling of the most expensive CCSD term is reduced to $V^2V_A^2O_A^2$ where V_A and O_A are the number of active virtual and occupied orbitals respectively. For some of the other CCSD terms arising from the double commutator, see Eq. (19) below, the scaling reduction is less favorable, but no terms scale worse than V^2O^2. This is less than the scaling of CC2 which is V^3O^2, so the overall scaling will be that of CC2 for large systems.

To divide the system, a localized set of molecular orbitals (MO) is generated and each orbital is assigned to an atom. Orbitals corresponding to active atoms then form an active orbital space while those corresponding to inactive atoms form an inactive space. We require that the orbitals are orthogonal and that the blocks of the Fock matrix corresponding to each space are diagonal. In this work, we have used Cholesky orbitals,[51] but other schemes are possible. After generating the orbital spaces, the cluster operator is divided into terms corresponding to each space, $X = T + S$, where T corresponds to the active space and S to the inactive. The approach can be generalized to several spaces.

The amplitude equations, Eq. 3, become

$$\langle \mu_1 | \, \hat{H} + [\hat{H}, X_2] \, | \mathrm{HF} \rangle = 0 \tag{18}$$

$$\langle \mu_2^T | \, \hat{H} + [\hat{H}, X_2] + \frac{1}{2}[[\hat{H}, X_2], X_2] \, | \mathrm{HF} \rangle = 0 \tag{19}$$

$$\langle \mu_2^S | \, [F, S_2] + \hat{H} + [\hat{H}, T_2] \, | \mathrm{HF} \rangle = 0. \tag{20}$$

In Eqs. (18)-(20), $\hat{H}$ refers to the X_1-transformed Hamiltonian operator

$$\hat{H} = \exp(-X_1) H \exp(X_1) \tag{21}$$

and μ^T and μ^S denote the active and inactive excited state manifolds, respectively. Note that the equations for the single amplitudes, Eq. (18), and active double amplitudes, Eq. (19), are the same as for full CCSD, while the equations for the inactive amplitudes, Eq. (20), are similar to those of CC2, but contain some extra terms involving the T-operator to give a balanced description. Excitations only involving active orbitals are referred to as internal while those only involving inactive orbitals are referred to as external. Excitations between the spaces are called semi external.

When calculating MLCCSD excitation energies, the equations are similar to those of full CCSD, however, the Jacobian matrix $\mathbf{A}$ is modified. The changes in the $\mathbf{A}$-matrix blocks are schematically summarized in Eq. (22) below

$$\mathbf{A}^{\mathrm{MLCCSD}} = \begin{array}{c} \\ T_1 \\ T_2 \\ S_2 \end{array} \begin{array}{c} \begin{array}{ccc} T_1 & T_2 & S_2 \end{array} \\ \begin{pmatrix} \mathrm{CCSD} & \mathrm{CCSD} & \mathrm{CCSD} \\ \mathrm{CCSD} & \mathrm{CCSD} & \mathrm{CCSD} \\ \mathrm{CCX} & \mathrm{CCX} & \mathrm{CC2} \end{pmatrix} \end{array} \tag{22}$$

The first two block rows, projecting against the singles and active doubles, are the same as for standard CCSD, while the lower right block is the same as in CC2 and is diagonal. Ideally, the CC2 block will have the largest dimension, resulting in a large reduction in computational cost compared to CCSD. The blocks labeled CCX in Eq. (22) contain hybrid terms between CC2 and CCSD that scales as CC2. For more details on MLCCSD linear response, see Ref. 44.

Similarly, the intensities can be found using either Eqs. (6)-(7) or Eq. (15), both involving the use of a MLCC-modified $\mathbf{F}$ matrix.[52] The $\mathbf{F}$ matrix can not be as easily divided into

blocks corresponding to the active and inactive space, but contains a mixture of terms that scale as CC2.

3 Results

3.1 General computational details

The MLCCSD approach for core excitation spectra has been implemented in a development version of the Dalton code.[53,54] As the current MLCCSD implementation is not optimized, our study has been limited to the relatively small molecules ethanal (acetaldehyde), propenal (acrolein) and butanal (butyraldehyde). Core absorption spectra have been computed using MLCCSD and compared to the corresponding full CCSD and CC2 spectra. As core-valence polarized basis sets are usually required for an accurate treatment of core excitations, we use aug-cc-pCVDZ basis set[55] for the atoms of the specific edges in ethanal and butanal, and either the aug-cc-pVDZ, indicated by aug-cc-p(C)VDZ, or the aug-cc-pCVDZ basis for the remaining atoms. Our results indicate that the difference in the results between these basis sets is negligible. Due to the high computational cost associated with the regular Lanczos algorithm, we only used aug-cc-pVDZ in the case of propenal.

The active spaces used are described for each case in the following subsections. We use the standard IUPAC numbering when discussing specific atoms, e.g. carbon 1 (C1) will always refer to the carbon closest to the oxygen atom, carbon 2 (C2) to the next carbon in the chain, and so on. Spectra are plotted using calculated excitation energies and oscillator strengths in the length gauge with an empirical line broadening of 1000 cm^{-1} and a normalized Lorentzian line shape function.

3.2 Ethanal

In Fig. 1, the active atoms of ethanal are colored red. Spaces **A**, **B** and **C** only contain one second row atom each, and they are the smallest active spaces possible. Our results indicate

that this is too small for some of the excitations we consider. Consequently we have also used space **D** that is the union of **A** and **B**.

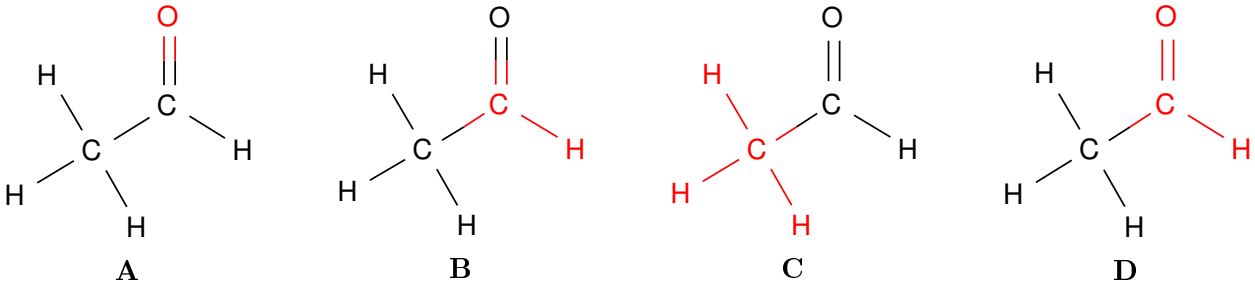

Figure 1: Active spaces of ethanal indicated in red.

The oxygen K-edge spectra calculated using the regular Lanczos algorithm with a chain length of 2000 are presented in Fig. 2a. The plots show the excitation energies and intensities calculated using CC2, CCSD, and MLCCSD with spaces **A** and **D**, employing aug-cc-pCVDZ for all models except MLCCSD **A**, where we used aug-cc-p(C)VDZ instead. For the main edge, both MLCCSD models agree almost perfectly with full CCSD. Model **A** is not able to reproduce the higher energy fine structure, while **D** is reasonably close. Both MLCCSD models, unlike CC2, reproduce the large gap between the main edge and the fine structure.

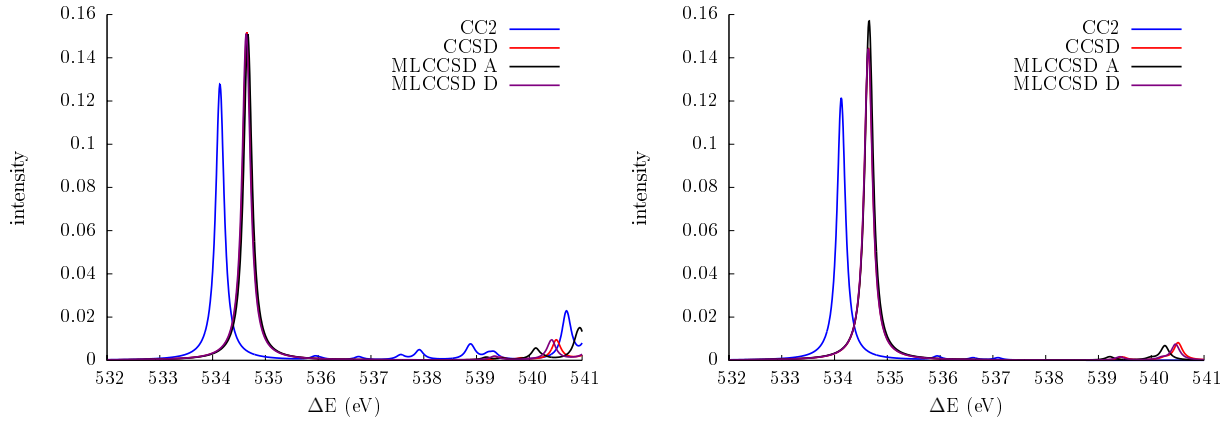

Figure 2: Ethanal. Comparison of the oxygen K-edge spectra as obtained in CC2, CCSD and MLCCSD using both the regular Lanczos algorithm (a) and the Davidson algorithm with the CVS approximation (b). Basis sets: aug-cc-p(C)VDZ for MLCCSD **A** and aug-cc-pCVDZ for the rest.

Figure 2b contains the equivalent spectra calculated using the CVS approximation within the standard implementation of CCLR. Note that only five excitations were calculated using each model. As a result, the spectra presented are not complete in the given energy range. This is particularly important for CC2 because the highest eigenvalue computed was at 537.10 eV. The excitation energies are collected in Table 1. Similar to the Lanczos case, the MLCCSD results are very good for the main edge and reasonably good for the fine structure. Unlike in the Lanczos case, model **A** overestimates the oscillator strength of the main edge by about 10%.

Table 1: Ethanal. Oxygen core excitation energies (in eV) and corresponding oscillator strengths $f \times 100$ (dimensionless, in parenthesis) computed using the CVS-Davidson algorithm. Basis sets: aug-cc-p(C)VDZ for MLCCSD **A** and aug-cc-pCVDZ for the rest.

	CC2	CCSD	MLCCSD **A**	MLCCSD **D**
S_1	534.13 (3.64)	534.64 (4.34)	534.65 (4.72)	534.64 (4.32)
S_2	535.95 (0.05)	539.46 (0.04)	539.21 (0.05)	539.40 (0.05)
S_3	536.62 (0.03)	540.25 (0.03)	539.99 (0.03)	540.20 (0.03)
S_4	536.83 (0.00)	540.50 (0.22)	540.26 (0.18)	540.46 (0.20)
S_5	537.10 (0.03)	540.56 (0.02)	540.28 (0.02)	540.49 (0.02)

The carbon K-edge spectra obtained using the regular Lanczos algorithm are plotted in Fig. 3. The main edge is well reproduced by MLCCSD **D**. For the higher excitations, however, MLCCSD seems to be closer to CC2. In should be noted that the Lanczos algorithm calculates all roots in this case, so the bands in Fig. 3 originate from both the active and inactive spaces. Furthermore, it is less straightforward to determine which excitations correspond to which individual core orbitals when using the Lanczos method without CVS.

These complications are lifted when applying, both in the Davidson and in Lanczos case, the CVS approximation as shown in Fig. 4. Note that the CC2 results are not included in the figure for clarity, but the values are reported in Table 2 and they are very similar to the Lanczos CC2 results. As the core orbitals are selected beforehand, it is possible to choose an active space corresponding to the relevant atom or atoms. From Fig. 4, we observe that MLCCSD **C** reproduces the carbon excitations of the methyl group very well. Model **B** has

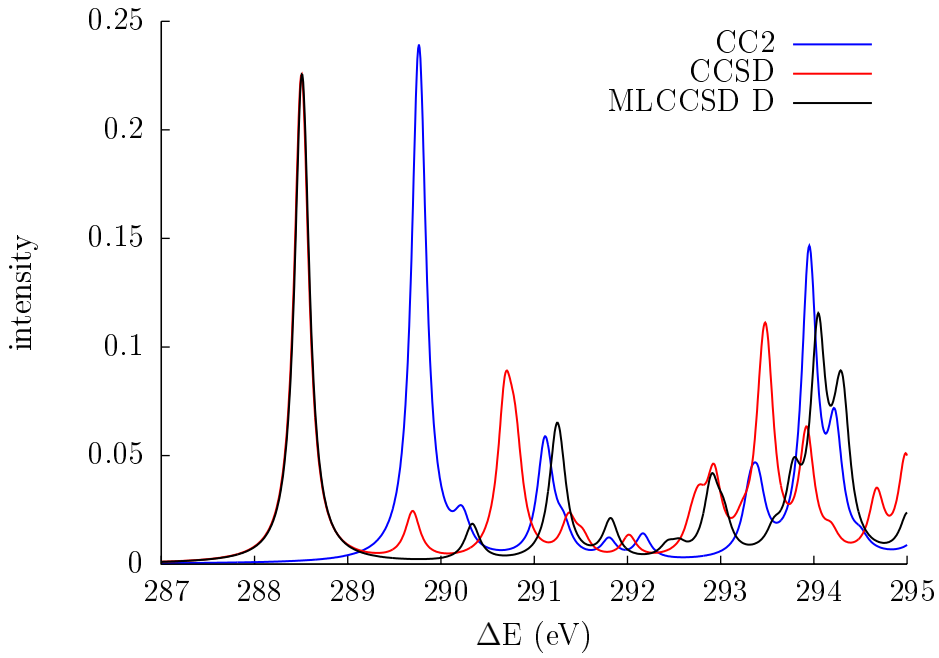

Figure 3: Ethanal. Comparison of the carbon K-edge spectrum as obtained in CC2, CCSD and MLCCSD via the regular Lanczos algorithm. Basis set aug-cc-pCVDZ.

a slightly shifted main edge, whereas **D** is almost indistinguishable from full CCSD.

Surprisingly, model **B** reproduces the peak just below 293 eV better than model **D**. Similar behavior is observed for the other molecules in this study. At these higher energies, the excitations have a higher double character and are more delocalized so the MLCCSD method is expected to be less successful. For this reason we believe the agreement with model **B** is a result of fortuitous error cancellation. Some of this may be due to the localized orbitals. Full CCSD is orbital invariant as long as there is no mixing of occupied and virtual orbitals. This invariance is broken by the CVS approximation and the Cholesky 1s orbital energy is about 0.04 eV higher than the canonical orbital energy in active space **B** while only 0.01 for active space **D**. These are small differences, but the effect is generally greater for smaller active spaces and basis sets.

To visualize the effect of the excitation process, we have plotted the change in the one-electron density between the ground and core excited states. This is achieved by calculating the orbital occupations in the two states and calculating the CCSD density difference using

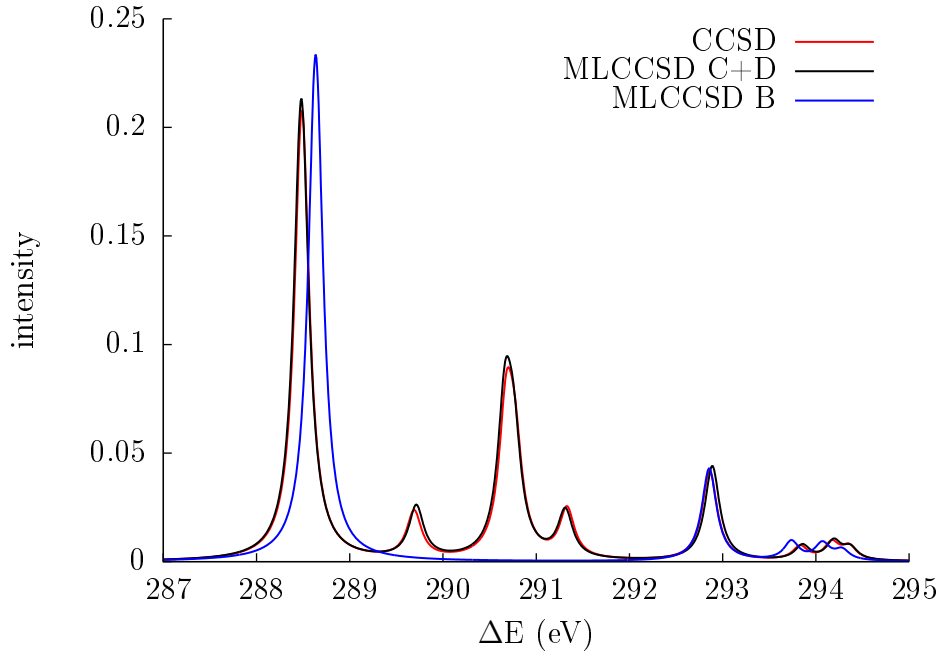

Figure 4: Ethanal. Comparison of the carbon K-edge spectrum as obtained in CC2, CCSD and MLCCSD using the CVS-Davidson algorithm. Basis sets: aug-cc-p(C)VDZ for MLCCSD **B** and aug-cc-pCVDZ for the rest.

Table 2: Ethanal. Carbon core excitation energies (eV) and corresponding oscillator strengths $f \times 100$ (dimensionless, in parentheses) computed using the CVS-Davidson algorithm. Basis sets: aug-cc-p(C)VDZ for MLCCSD **B** and aug-cc-pCVDZ for the rest.

		CC2	CCSD	MLCCSD **C**+**D**	MLCCSD **B**
C1	S_1	289.74 (6.63)	288.49 (6.23)	288.48 (6.38)	288.63 (7.00)
	S_2	293.48 (0.84)	292.86 (1.24)	292.89 (1.31)	292.86 (1.28)
	S_3	294.23 (0.21)	293.83 (0.19)	293.86 (0.20)	293.74 (0.26)
	S_4	294.54 (0.14)	294.17 (0.24)	294.19 (0.26)	294.07 (0.23)
	S_5	294.76 (0.12)	294.36 (0.19)	294.37 (0.17)	294.28 (0.14)
C2	S_1	290.15 (0.01)	289.55 (0.00)	289.52 (0.00)	-
	S_2	290.21 (0.49)	289.69 (0.64)	289.71 (0.72)	-
	S_3	291.10 (1.23)	290.68 (1.95)	290.67 (2.03)	-
	S_4	291.12 (0.57)	290.77 (1.22)	290.76 (1.34)	-
	S_5	291.66 (0.52)	291.33 (0.68)	291.31 (0.65)	-

Molden.[56] In Fig. 5 the density difference in the molecular plane is plotted for the most intense peaks of each atom in ethanal. Immediately noticeable is the very large reduction in the core density of the atom being excited and a corresponding increase in the density around the core. Furthermore, the oxygen excitation is highly localized with almost all the change taking place on the oxygen atom, and only a small change on C1. The carbon excitations are also fairly localized, but less so than for oxygen, particularly for C1.

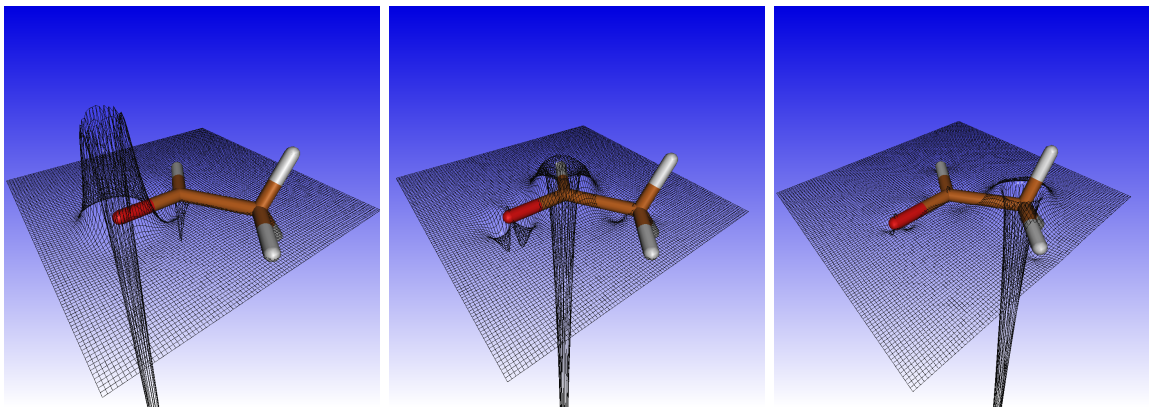

Figure 5: Difference in excited and ground state electron density in the molecular plane for the most intense peaks of oxygen (left), C1 (middle) and C2 (right) calculated at the CCSD level.

Figure 6 shows the same excitations plotted as 3D isosurfaces. Blue surfaces correspond to increased densities and red to decreased densities. This reveals that most of the increase goes out of the molecular plane for C1 and oxygen. Analysis of the excitation vector reveals that the excitations are indeed 1s $\rightarrow \pi^*$ excitations. The excitation from C2 is also a 1s $\rightarrow \pi^*$ excitation, but it is less clear from the density change. The greater localization for oxygen and C2 can explain why MLCCSD **A** and **C** perform better for these atoms than MLCCSD **B** does for C1.

3.3 Propenal

Propenal is the smallest conjugated aldehyde and we will use it to study the performance of MLCCSD for a conjugated system. The active spaces adopted are summarized in Fig. 7.

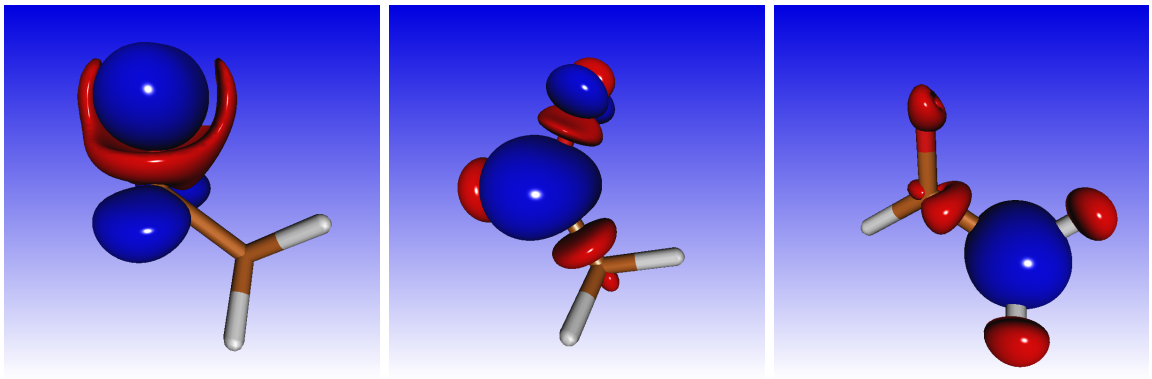

Figure 6: Difference in excited and ground state electron density plotted as isosurfaces (0.01) for the most intense peaks of oxygen (left), C1 (middle) and C2 (right) calculated with CCSD. Blue corresponds to increased and red to decreased density.

Spaces **A** to **D** only contain one second row element each, while **E** and **F** contain a double bond each.

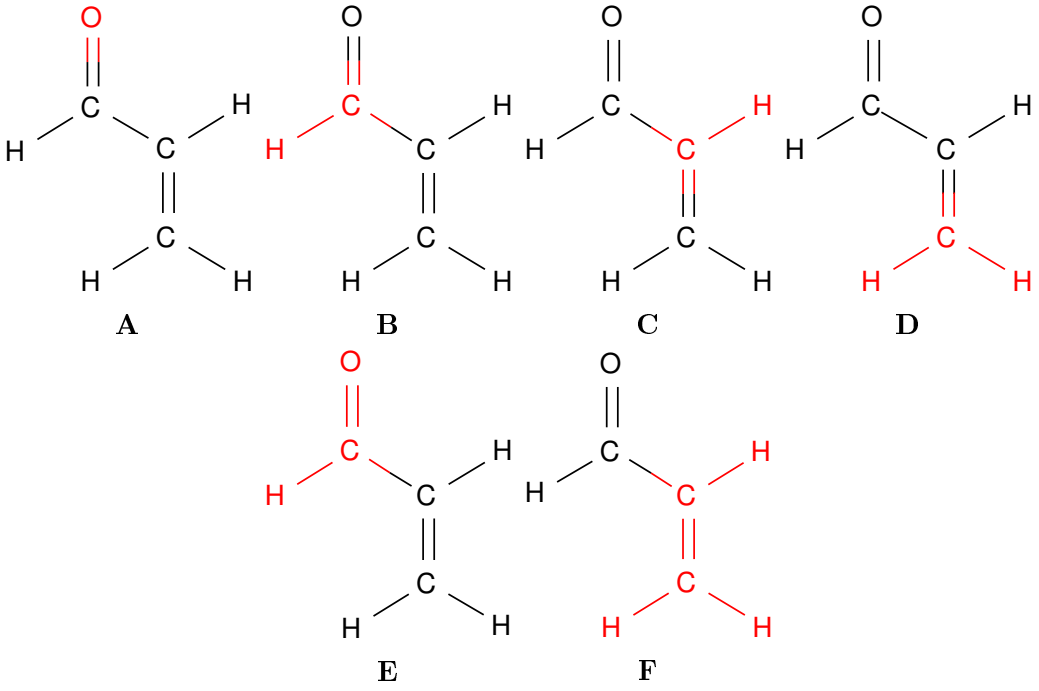

Figure 7: Active spaces of propenal in red

The CVS Davidson results for oxygen are presented in Fig. 8 and Table 3. As for ethanal, both spaces containing oxygen reproduce the main edge well, and **E** is better for the fine structure. Again, CC2 fails and yields too small a gap between the main edge and the next excitation.

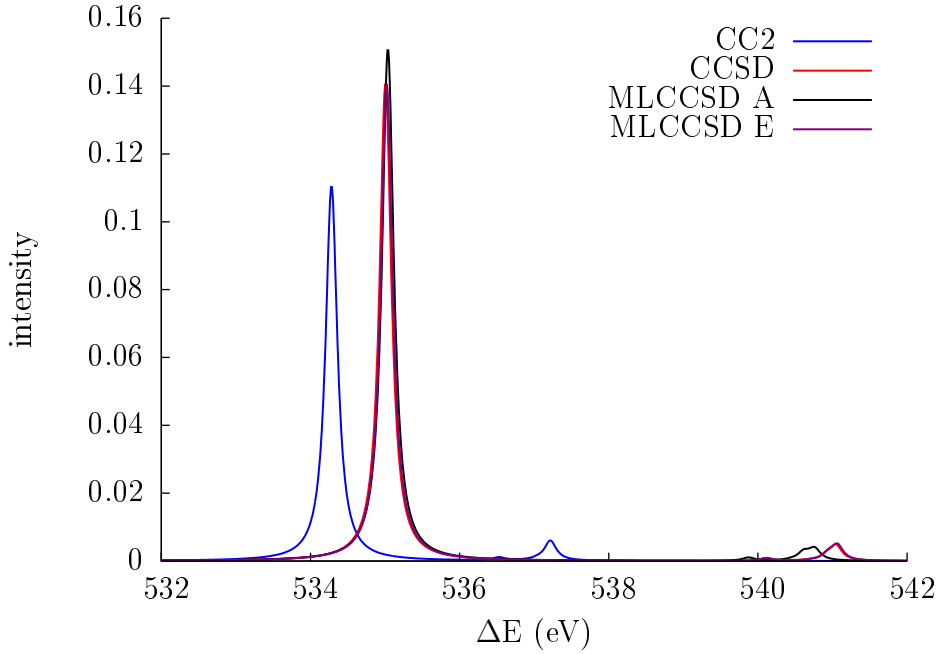

Figure 8: Propenal. Comparison of the oxygen K-edge spectra obtained with CC2, CCSD, and MLCCSD **A** and **E** and the CVS-Davidson algorithm. Basis set: aug-cc-pVDZ.

Table 3: Propenal. Oxygen CVS-Davidson core excitation energies (eV) and corresponding oscillator strengths $f \times 100$ (dimensionless, in parentheses). Basis set: aug-cc-pVDZ.

	CC2	CCSD	MLCCSD **A**	MLCCSD **E**
S_1	534.28 (3.31)	535.01 (4.22)	535.04 (4.53)	535.02 (4.22)
S_2	536.53 (0.03)	540.11 (0.02)	539.87 (0.03)	540.12 (0.02)
S_3	537.05 (0.01)	540.71 (0.00)	540.45 (0.01)	540.72 (0.00)
S_4	537.22 (0.17)	540.93 (0.05)	540.61 (0.07)	540.94 (0.05)
S_5	537.29 (0.00)	541.05 (0.13)	540.76 (0.10)	541.06 (0.14)

Obtaining the carbon K-edge spectrum in propenal is more complicated than for ethanal because there are more carbon atoms. Combining the regular Lanczos algorithm with ML-CCSD would produce a large number of peaks corresponding to inactive atoms and make the spectrum very difficult to interpret. In Fig. 9 we compare the CCSD and CC2 spectra obtained with the CVS-Davidson algorithm and to the CCSD regular Lanczos spectrum. While CC2 performs better for carbon than for oxygen, there are still large discrepancies compared to CCSD. Comparing the Lanczos and CVS algorithms, we generally find a good agreement below 292 eV, though with some small differences. These differences may be due to the Lanczos algorithm not being fully converged for the chosen chain length of 3000. Above 292 eV, the two spectra differ significantly. This happens because there is a large number of states in this energy range and only five roots for each C atom were determined using the CVS-Davidson approach. Consequently, only few states were obtained within this energy range and it was somewhat arbitrary which states the Davidson algorithm converged to. Because CCSD and MLCCSD use different orbitals, the two methods will often converge to different roots in such cases. This complication can be avoided by calculating more states. The CVS results for CC2 and CCSD, as well as for two sets of MLCCSD active spaces, are reported in Table 4.

In Fig. 10a, the same CVS CCSD spectrum is compared to a MLCCSD spectrum computed using the minimal active spaces **B**, **C** and **D**. MLCCSD reproduces the main features of the spectrum and for most applications this will be sufficiently accurate. Figure 10b is similar to Fig. 10a, but a set of larger active spaces was used in the MLCCSD calculation. Spaces **E** and **F** both contain two second row atoms, **E** contains oxygen and C1 and **F** contains the remaining carbons. As can be seen in the figure, this gives excellent results for the excitations below 293 eV. Note that the peak at 287.5 eV appears to be a bit too intense. This happens because the peak is the sum of two excitations that are separated by 0.07 eV in the CCSD case and by 0.03 eV in MLCCSD, see Table 4. The calculated intensities are actually slightly lower for MLCCSD.

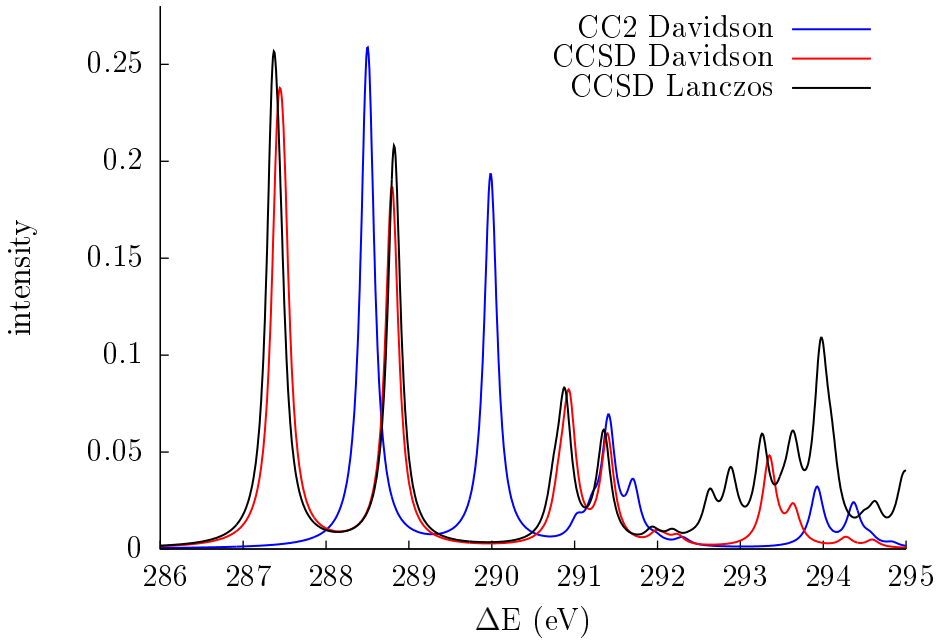

Figure 9: Propenal. Comparison of the carbon K-edge spectra obtained with the CVS-Davidson and regular Lanczos algorithms. Basis set: aug-cc-pVDZ.

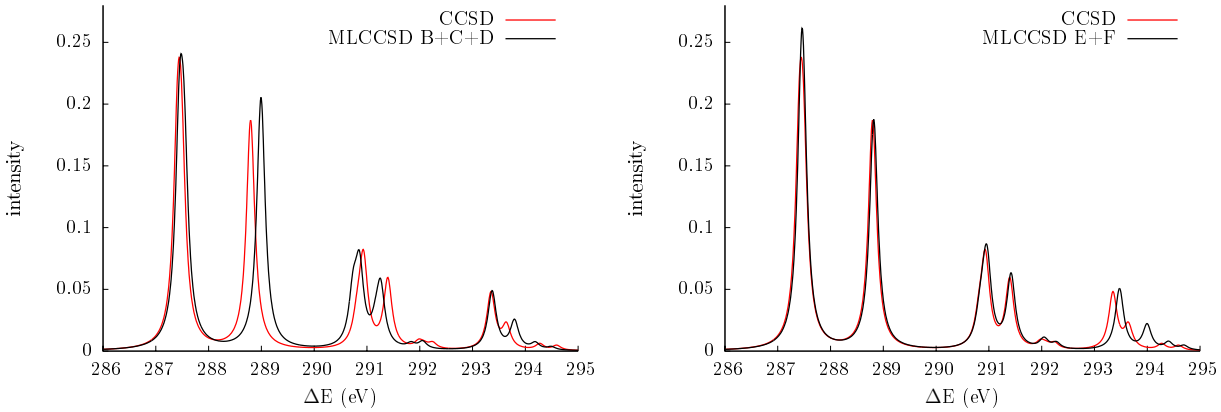

Figure 10: Propenal. Comparison of the carbon K-edge spectra obtained with CCSD and MLCCSD **B**, **C** and **D** (a) and **E** and **F** (b) with the CVS-Davidson algorithm. Basis: set aug-cc-pVDZ.

Table 4: Propenal. Carbon CVS-Davidson core excitation energies (eV) and corresponding oscillator strengths $f \times 100$ (dimensionless, in parentheses). Basis set: aug-cc-pVDZ.

		CC2	CCSD	**B**+**C**+**D**	**E**+**F**
C1	S_1	289.99 (5.76)	288.80 (5.56)	288.99 (6.11)	288.82 (5.58)
	S_2	293.93 (0.92)	293.35 (1.38)	293.37 (1.42)	293.47 (1.49)
	S_3	294.37 (0.65)	293.64 (0.56)	293.79 (0.69)	294.00 (0.60)
	S_4	294.56 (0.12)	294.27 (0.15)	294.19 (0.16)	294.40 (0.18)
	S_5	294.83 (0.06)	294.59 (0.11)	294.49 (0.07)	294.70 (0.10)
C2	S_1	288.52 (3.50)	287.48 (3.75)	287.54 (3.66)	287.48 (3.67)
	S_2	291.03 (0.29)	290.91 (0.71)	290.74 (0.65)	290.91 (0.74)
	S_3	291.41 (1.66)	290.94 (1.50)	290.86 (1.84)	290.97 (1.73)
	S_4	291.41 (0.21)	291.41 (0.16)	291.17 (0.36)	291.41 (0.24)
	S_5	291.97 (0.08)	292.08 (0.07)	291.84 (0.06)	292.07 (0.07)
C3	S_1	288.49 (4.40)	287.41 (4.32)	287.45 (4.85)	287.45 (4.31)
	S_2	291.22 (0.37)	290.81 (0.53)	290.73 (0.53)	290.83 (0.54)
	S_3	291.71 (0.85)	291.39 (1.51)	291.26 (1.41)	291.42 (1.53)
	S_4	292.27 (0.02)	291.98 (0.16)	291.83 (0.06)	292.03 (0.18)
	S_5	292.31 (0.10)	292.24 (0.14)	292.05 (0.18)	292.28 (0.14)

3.4 Butanal

Finally, to investigate the behavior of single bonded carbon chains we calculated the core excitation energies of butanal.[57] We used the active spaces in Fig. 11. Active space **A** contains the oxygen atom and the attached methine group which proved sufficient for ethanal and propenal. The active spaces **B**, **C** and **D** only contain a methyl or a methylene group.

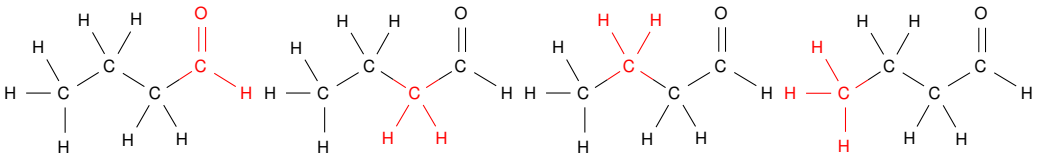

A **B** **C** **D**

Figure 11: Active spaces of butanal in red.

Figure 12 shows the spectra at the oxygen K-edge of butanal calculated with CC2, CCSD and MLCCSD and the CVS-Davidson algorithm. Similarly to ethanal and propenal, the excitation energy of the main edge is too low with CC2 and the gap to the higher shake-up

excitations is too small. The spectra for CCSD and MLCCSD are almost indistinguishable, even for the higher excitations.

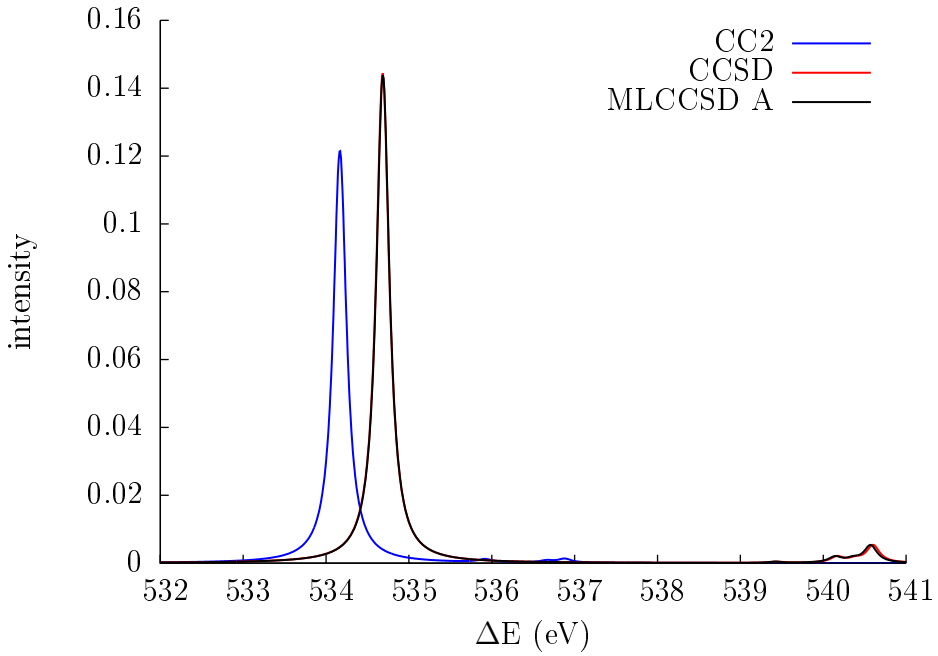

Figure 12: Butanal. CVS-Davidson oxygen K-edge calculated with the Davidson algorithm. Basis set: aug-cc-pCVDZ

Table 5 collects the core excitation energies of oxygen in butanal with the corresponding oscillator strengths. None of the errors in the MLCCSD energies compared to CCSD are larger than 0.03 eV. The errors in the oscillator strengths are also small, whereas the relative errors vary a lot because the magnitude of the oscillator strengths vary by three orders of magnitude.

Table 5: Butanal. Oxygen CVS-Davidson core excitation energies (eV) and corresponding oscillator strengths $f \times 100$ (dimensionless, in parentheses). Basis set: aug-cc-pCVDZ.

	CC2	CCSD	MLCCSD **A**
S_1	534.17 (3.65)	534.68 (4.33)	534.69 (4.31)
S_2	535.92 (0.03)	539.44 (0.01)	539.42 (0.01)
S_3	536.66 (0.01)	540.17 (0.05)	540.14 (0.05)
S_4	536.68 (0.00)	540.39 (0.03)	540.36 (0.03)
S_5	536.88 (0.03)	540.60 (0.15)	540.57 (0.15)

Obtaining the carbon K-edge spectrum requires a bit more care in the choice of active space, depending on the accuracy required. In Fig. 13, the peaks below 289 eV and above 292 eV correspond to C1 and were calculated using active space **A** in MLCCSD and these are well reproduced. The rest of the peaks are from the atoms C2, C3 and C4. They are shifted down a bit compared to CCSD, but overall correspond reasonably well with CCSD. The CC2 spectrum is omitted from Fig. 13 for clarity, but it showed similar discrepancies from CCSD as seen in ethanal and propenal.

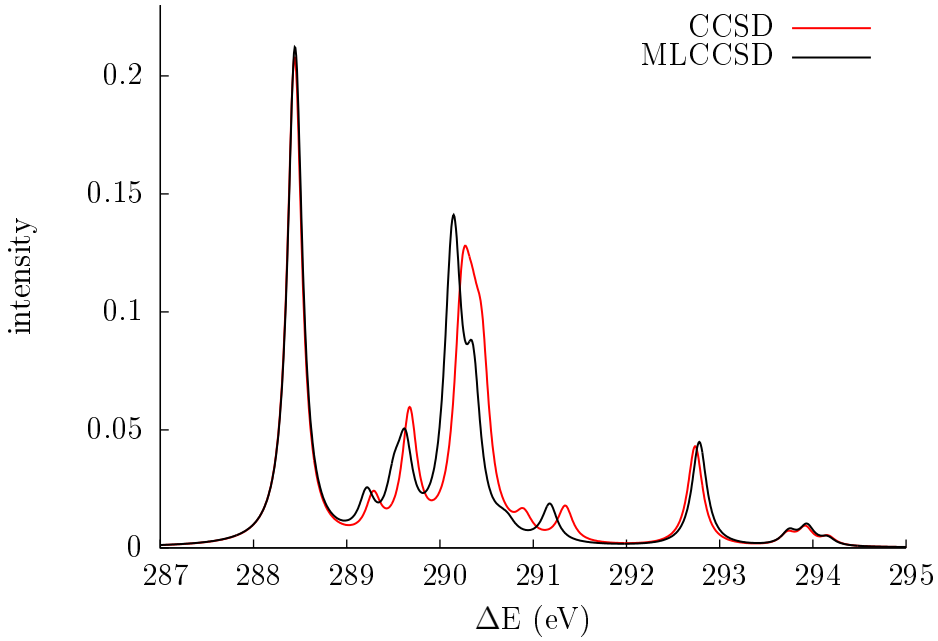

Figure 13: Butanal. CVS-Davidson carbon K-edge calculated with the Davidson algorithm. Basis set: aug-cc-pCVDZ

Comparing the excitation energies in Tab. 6, the largest error for C1 is about 0.04 eV. For the other carbons, the errors are larger, but none are larger than 0.3 eV. We note that in some cases, the CC2 excitation energies are more accurate than the MLCCSD excitation energies. These are weak excitations that will be difficult to see in an experiment and oscillator strengths are better described by MLCCSD.

Table 6: Butanal. Carbon CVS-Davidson core excitation energies (eV) and corresponding oscillator strengths $f \times 100$ (dimensionless, in parenthesis). Basis set aug-cc-pCVDZ.

		CC2	CCSD	MLCCSD
C1	S_1	289.70 (6.59)	288.44 (6.21)	288.44 (6.33)
	S_2	293.34 (0.86)	292.74 (1.27)	292.78 (1.33)
	S_3	294.16 (0.14)	293.73 (0.15)	293.74 (0.17)
	S_4	294.25 (0.13)	293.92 (0.22)	293.94 (0.24)
	S_5	294.43 (0.09)	294.16 (0.11)	294.16 (0.09)
C2	S_1	290.04 (0.11)	289.52 (0.01)	289.46 (0.02)
	S_2	290.08 (0.62)	289.68 (1.01)	289.63 (1.05)
	S_3	290.75 (0.98)	290.45 (1.78)	290.35 (1.76)
	S_4	290.96 (0.08)	290.88 (0.17)	290.73 (0.13)
	S_5	291.28 (0.02)	291.30 (0.03)	291.12 (0.02)
C3	S_1	289.93 (0.35)	289.66 (0.60)	289.51 (0.55)
	S_2	290.51 (0.07)	290.35 (1.25)	290.16 (1.19)
	S_3	290.52 (0.55)	290.54 (0.06)	290.28 (0.10)
	S_4	290.80 (0.01)	290.91 (0.07)	290.61 (0.01)
	S_5	290.84 (0.05)	290.93 (0.05)	290.65 (0.08)
C4	S_1	289.70 (0.38)	289.29 (0.50)	289.21 (0.51)
	S_2	290.48 (0.78)	290.22 (1.45)	290.11 (1.44)
	S_3	290.51 (0.71)	290.27 (1.47)	290.16 (1.43)
	S_4	290.80 (0.00)	290.68 (0.02)	290.55 (0.01)
	S_5	291.36 (0.35)	291.35 (0.43)	291.18 (0.46)

Table 7: Ethanal. Oxygen core excitation energies (in eV) and corresponding oscillator strengths $f \times 100$ (dimensionless, in parenthesis) computed using the CVS-Davidson algorithm compared with experiment[58] Basis sets: aug-cc-pCVTZ.

	CC2	CCSD	MLCCSD **A**	MLCCSD **D**	Experiment
S_1	532.58 (3.85)	532.69 (4.42)	0.00 (0.00)	0.00 (0.00)	531.53
S_2	534.61 (0.05)	537.50 (0.04)	0.00 (0.00)	0.00 (0.00)	535.42
S_3	535.27 (0.02)	538.28 (0.02)	0.00 (0.00)	0.00 (0.00)	536.32
S_4	535.43 (0.00)	538.52 (0.22)	0.00 (0.00)	0.00 (0.00)	537.05

Table 8: Ethanal. Relative oxygen core excitation energies (in eV) computed using the CVS-Davidson algorithm compared with experiment[58] Basis sets: aug-cc-pCVTZ.

	CC2	CCSD	Experiment
S_1	0.00	0.00	0.00
S_2	2.03	4.82	3.89
S_3	2.69	5.59	4.79
S_4	2.85	5.83	5.52

3.5 Comparison with experiment

4 Conclusions

With the examples presented in this paper, we have demonstrated that it is possible to determine CCSD core excitation energies and oscillator strengths using MLCCSD with small active spaces. In many cases, the results obtained with the smallest active spaces are sufficiently accurate given that a linewidth of 1 eV or more is not uncommon in experiments.[58] Small expansions of the active spaces in ethanal and propenal were sufficient to obtain CCSD results with errors less than 0.01 eV.

The current implementation is not yet fully optimal for production calculations and no timings are therefore reported in this paper. However, the most expensive term in CCSD scales as V^4O^2, while CC2 scales as V^3O^2. Butanal is a quite small molecule and with active space **A**, the most expensive term to calculate in MLCCSD will be the same as in full CCSD. The theoretical time reduction in the CCSD part is

$$\frac{V^4O^2}{V^2V_A^2O_A^2} = \frac{187^2 \times 20^2}{61^2 \times 8^2} \approx 59 \tag{23}$$

and the overall theoretical scaling is that of CC2. Actual time reduction will depend on the implementation and size of the active part compared to the whole system, but results with multi-level CC3[59] indicate that time reductions are close to the theoretical value for sufficiently large systems.

To further investigate the excitation processes, we have visualized the change in electronic density between states. For core excitations, a large reduction of electronic density is observed in the core and a corresponding increase in the valence region. This may be used to determine a suitable active space. If the electron change is delocalized with a low level method, a larger active space may be required. For small active spaces that only contain one second row atom, increasing the size will probably not appreciably affect the overall computational cost because the inactive part is relatively more expensive. Systematic studies with different spaces will give an indication on whether the active space is large enough.

Acknowledgement

H.K. and R.H.M. thank T. J. Martinez for hosting part of this project at Stanford University. H.K. acknowledges financial support from the FP7-PEOPLE-2013-IOF funding scheme (Project No. 625321). S.C. acknowledges financial support from the AIAS-COFUND program (Grant Agreement No. 609033). The COST Actions No. CM1002 "COnvergent Distributed Environment for Computational Spectroscopy (CODECS)", MP1306 "Modern Tools for Spectroscopy on Advanced Materials (EUSPEC)" and CM1204 "XUV/X-ray light and fast ions for ultrafast chemistry (XLIC)" are also acknowledged.

Supporting Information Available

Molecular geometries used in the calculations are available as additional information.

This material is available free of charge via the Internet at `http://pubs.acs.org/`.

References

(1) Holch, F.; Hübner, D.; Fink, R.; Schöll, A.; Umbach, E. *J. Electron Spectrosc.* **2011**, *184*, 452 – 456.

(2) Garino, C.; Borfecchia, E.; Gobetto, R.; van Bokhoven, J. A.; Lamberti, C. *Coordin. Chem. Rev.* **2014**, *277*, 130 – 186, Following Chemical Structures using Synchrotron Radiation.

(3) Petrović, V. S.; Siano, M.; White, J. L.; Berrah, N.; Bostedt, C.; Bozek, J. D.; Broege, D.; Chalfin, M.; Coffee, R. N.; Cryan, J.; Fang, L.; Farrell, J. P.; Frasinski, L. J.; Glownia, J. M.; Gühr, M.; Hoener, M.; Holland, D. M. P.; Kim, J.; Marangos, J. P.; Martinez, T.; McFarland, B. K.; Minns, R. S.; Miyabe, S.; Schorb, S.; Sension, R. J.; Spector, L. S.; Squibb, R.; Tao, H.; Underwood, J. G.; Bucksbaum, P. H. *Phys. Rev. Lett.* **2012**, *108*, 253006.

(4) McFarland, B. K.; Farrell, J. P.; Miyabe, S.; Tarantelli, F.; Aguilar, A.; Berrah, N.; Bostedt, C.; Bozek, J. D.; Bucksbaum, P. H.; Castagna, J. C.; Coffee, R. N.; Cryan, J. P.; Fang, L.; Feifel, R.; Gaffney, K. J.; Glownia, J. M.; Martinez, T. J.; Mucke, M.; Murphy, B.; Natan, A.; Osipov, T.; Petrović, V. S.; Schorb, S.; Schultz, T.; Spector, L. S.; Swiggers, M.; Tenney, I.; Wang, S.; White, J. L.; White, W.; Gühr, M. *Nat. Commun.* **2014**, *5*, 4235.

(5) Liekhus-Schmaltz, C. E.; Tenney, I.; Osipov, T.; Sanchez-Gonzalez, A.; Berrah, N.; Boll, R.; Bomme, C.; Bostedt, C.; Bozek, J. D.; Carron, S.; Coffee, R.; Devin, J.; Erk, B.; Ferguson, K. R.; Field, R. W.; Foucar, L.; Frasinski, L. J.; Glownia, J. M.; Gühr, M.; Kamalov, A.; Krzywinski, J.; Li, H.; Marangos, J. P.; Martinez, T. J.; McFarland, B. K.; Miyabe, S.; Murphy, B.; Natan, A.; Rolles, D.; Rudenko, A.; Siano, M.; Simpson, E. R.; Spector, L.; Swiggers, M.; Walke, D.; Wang, S.; Weber, T.; Bucksbaum, P. H.; Petrović, V. S. *Nat. Commun.* **2015**, *6*, 8199.

(6) Plekan, O.; Feyer, V.; Richter, R.; Coreno, M.; de Simone, M.; Prince, K.; Trofimov, A.; Gromov, E.; Zaytseva, I.; Schirmer, J. *Chem. Phys.* **2008**, *347*, 360–375.

(7) Feyer, V.; Plekan, O.; Richter, R.; Coreno, M.; de Simone, M.; Prince, K. C.; Trofimov, A. B.; Zaytseva, I. L.; Schirmer, J. *J. Phys. Chem. A* **2010**, *114*, 10270âĂŞ10276.

(8) Davidson, E. J. *J. Comp. Phys.* **1975**, *17*, 87–94.

(9) Crouzeix, M.; Philippe, B.; Sadkane, M. *SIAM J. Sci. Comput.* **1994**, *15*, 62–76.

(10) Slater, J. C. In *Statistical Exchange-Correlation in the Self-Consistent Field*; Löwdin, P.-O., Ed.; Adv. Quant. Chem.; Academic Press, 1972; Vol. 6; pp 1 – 92.

(11) Slater, J. C.; Johnson, K. H. *Phys. Rev. B* **1972**, *5*, 844–853.

(12) Stener, M.; Lisini, A.; Decleva, P. *Chem. Phys.* **1995**, *191*, 141 – 154.

(13) Triguero, L.; Pettersson, L. G. M.; Ågren, H. *Phys. Rev. B* **1998**, *58*, 8097–8110.

(14) Natoli, C. R.; Misemer, D. K.; Doniach, S.; Kutzler, F. W. *Phys. Rev. A* **1980**, *22*, 1104–1108.

(15) Fonda, L. *J. Phys.: Condens. Mat.* **1992**, *4*, 8269.

(16) Ankudinov, A. L.; Ravel, B.; Rehr, J. J.; Conradson, S. D. *Phys. Rev. B* **1998**, *58*, 7565–7576.

(17) Schwerdtfeger, P. *ChemPhysChem* **2011**, *12*, 3143–3155.

(18) Taillefumier, M.; Cabaret, D.; Flank, A.-M.; Mauri, F. *Phys. Rev. B* **2002**, *66*, 195107.

(19) Bagus, P. S. *Phys. Rev.* **1965**, *139*, A619–A634.

(20) Meehan, T. E.; Hermann, K.; Larkins, F. P. *J. Phys. B: At. Mol. Opt.* **1995**, *28*, 357.

(21) Ekström, U.; Norman, P.; Carravetta, V.; Ågren, H. *Phys. Rev. Lett.* **2006**, *97*, 143001.

(22) Ekström, U.; Norman, P. *Phys. Rev. A* **2006**, *74*, 042722.

(23) Besley, N. A.; Asmuruf, F. A. *Phys. Chem. Chem. Phys.* **2010**, *12*, 12024–12039.

(24) Stener, M.; Fronzoni, G.; de Simone, M. *Chem. Phys. Lett.* **2003**, *373*, 115 – 123.

(25) Zhang, Y.; Biggs, J. D.; Healion, D.; Govind, N.; Mukamel, S. *J. Chem. Phys.* **2012**, *137*.

(26) Cederbaum, L. S.; Domcke, W.; Schirmer, J. *Phys. Rev. A* **1980**, *22*, 206–222.

(27) Schirmer, J. *Phys. Rev. A* **1982**, *26*, 2395–2416.

(28) Wormit, M.; Rehn, D. R.; Harbach, P. H.; Wenzel, J.; Krauter, C. M.; Epifanovsky, E.; Dreuw, A. *Mol. Phys.* **2014**, *112*, 774–784.

(29) Wenzel, J.; Wormit, M.; Dreuw, A. *J. Comput. Chem.* **2014**, *35*, 1900–1915.

(30) Wenzel, J.; Holzer, A.; Wormit, M.; Dreuw, A. *J. Chem. Phys.* **2015**, *142*.

(31) Wenzel, J.; Wormit, M.; Dreuw, A. *J. Chem. Theory Comput.* **2014**, *10*, 4583–4598.

(32) Schirmer, J.; Trofimov, A. B. *J. Chem. Phys.* **2004**, *120*, 11449–11464.

(33) Trofimov, A.; Krivdina, I.; Weller, J.; Schirmer, J. *Chem. Phys.* **2006**, *329*, 1 – 10.

(34) Nooijen, M.; Bartlett, R. J. *J. Chem. Phys.* **1995**, *102*, 6735–6756.

(35) Coriani, S.; Fransson, T.; Christiansen, O.; Norman, P. *J Chem. Theory Comput.* **2012**, *8*, 1616–1628.

(36) Coriani, S.; Christiansen, O.; Fransson, T.; Norman, P. *Phys. Rev. A* **2012**, *85*, 022507.

(37) Fransson, T.; Coriani, S.; Christiansen, O.; Norman, P. *J. Chem. Phys.* **2013**, *138*.

(38) List, N. H.; Coriani, S.; Kongsted, J.; Christiansen, O. *J. Chem. Phys.* **2014**, *141*.

(39) Coriani, S.; Koch, H. *J. Chem. Phys.* **2015**, *143*, 181103.

(40) Kauczor, J.; Norman, P.; Christiansen, O.; Coriani, S. *J. Chem. Phys.* **2013**, *139*, 211102.

(41) Peng, B.; Lestrange, P. J.; Goings, J. J.; Caricato, M.; Li, X. *J. Chem. Theory Comp.* **2015**, *11*, 4146–4153, PMID: 26575909.

(42) Golub, G. H.; Van Loan, C. F. *Matrix Computations*, 3rd ed.; Johns Hopkins University Press: Philadelphia, PA, 1996.

(43) Myhre, R. H.; Sánchez de Merás, A. M. J.; Koch, H. *Mol. Phys.* **2013**, *111*, 1109–1118.

(44) Myhre, R. H.; Sánchez de Merás, A. M. J.; Koch, H. *J. Chem. Phys.* **2014**, *141*, –.

(45) Koch, H.; Jørgensen, P. *J. Chem. Phys.* **1990**, *93*, 3333–3344.

(46) Christiansen, O.; Jørgensen, P.; Hättig, C. *Int. J. Quantum Chem.* **1997**, *68*, 1–52.

(47) Lanczos, C. *J. Res. Nat. Bur. Stand.* **1950**, *45*, 225–282.

(48) Meyer, H.; Pal, S. *J. Chem. Phys.* **1989**, *91*, 6195–6204.

(49) Purvis, G. D.; Bartlett, R. J. *J. Chem. Phys.* **1982**, *76*, 1910.

(50) Christiansen, O.; Koch, H.; Jørgensen, P. *Chem. Phys. Lett.* **1995**, *243*, 409–418.

(51) de Merás, A. M. J. S.; Koch, H.; Cuesta, I. G.; Boman, L. *J. Chem. Phys.* **2010**, *132*, 204105.

(52) Skjelbred, K. M.; Myhre, R. H.; Koch, H. in preparation.

(53) Aidas, K.; Angeli, C.; Bak, K. L.; Bakken, V.; Bast, R.; Boman, L.; Christiansen, O.; Cimiraglia, R.; Coriani, S.; Dahle, P.; Dalskov, E. K.; Ekström, U.; Enevoldsen, T.; Eriksen, J. J.; Ettenhuber, P.; Fernández, B.; Ferrighi, L.; Fliegl, H.; Frediani, L.; Hald, K.; Halkier, A.; Hättig, C.; Heiberg, H.; Helgaker, T.; Hennum, A. C.; Hettema, H.; Hjertenæs, E.; Høst, S.; Høyvik, I.-M.; Iozzi, M. F.; Jansík, B.; Jensen, H. J. A.; Jonsson, D.; Jørgensen, P.; Kauczor, J.; Kirpekar, S.; Kjærgaard, T.; Klopper, W.; Knecht, S.; Kobayashi, R.; Koch, H.; Kongsted, J.; Krapp, A.; Kristensen, K.;

Ligabue, A.; Lutnæs, O. B.; Melo, J. I.; Mikkelsen, K. V.; Myhre, R. H.; Neiss, C.; Nielsen, C. B.; Norman, P.; Olsen, J.; Olsen, J. M. H.; Osted, A.; Packer, M. J.; Pawlowski, F.; Pedersen, T. B.; Provasi, P. F.; Reine, S.; Rinkevicius, Z.; Ruden, T. A.; Ruud, K.; Rybkin, V. V.; Sałek, P.; Samson, C. C. M.; de Merás, A. S.; Saue, T.; Sauer, S. P. A.; Schimmelpfennig, B.; Sneskov, K.; Steindal, A. H.; Sylvester-Hvid, K. O.; Taylor, P. R.; Teale, A. M.; Tellgren, E. I.; Tew, D. P.; Thorvaldsen, A. J.; Thøgersen, L.; Vahtras, O.; Watson, M. A.; Wilson, D. J. D.; Ziolkowski, M.; Ågren, H. *Wiley Interdiscip. Rev. Comput. Mol. Sci.* **2014**, *4*, 269–284.

(54) Dalton, a molecular electronic structure program, Release Dalton2016. 2015; `http://daltonprogram.org/`.

(55) Woon, D. E.; Dunning, T. H. *J. Chem. Phys.* **1995**, *103*, 4572–4585.

(56) G.Schaftenaar,; Noordik, J. *J. Comput.-Aided Mol. Design* **2000**, *14*, 123–134.

(57) National Center for Biotechnology Information. Pubchem Compound Database. `https://pubchem.ncbi.nlm.nih.gov/compound/261`, accessed January 2016; CID = 261.

(58) Prince, K. C.; Richter, R.; De Simone, M.; Coreno, M. *Surf. Rev. Lett.* **2002**, *09*, 159–164.

(59) Myhre, R. H.; Koch, H. in preparation.

Graphical TOC Entry